# POSTBUCKLING CHARACTERISTICS OF THE SHORT SUPERELASTIC SHAPE MEMORY ALLOY COLUMNS- EXPERIMENT AND QUANTITATIVE ANALYSIS

M.A. RAHMAN[*]
Department of Mechanical Engineering
Bangladesh University of Engineering & Technology
Dhaka 1000, BANGLADESH
e-mail: ashiq@me.buet.ac.bd


J. TANI
Institute of Fluid Science, Tohoku University
Katahira 2-1-1, Aoba-ku, Sendai-shi 980-8577, JAPAN

A few unique buckling and postbuckling characteristics of short superelastic shape memory alloy (SMA) columns are observed experimentally and explained in terms of numerical simulation. Interestingly, it is found from the load-deformation curves that during compression the SMA column with slenderness ratio $(L/k)$ of 38 exhibits two distinct buckling loads, the other one being higher, completely contrary to the general notion that load falls off monotonously for all columns in the postbuckling region. Similarly, for $L/k$ of 28, the SMA column can sustain a significantly high load after a distinct change in the mode of deformation. Based on the large deformation theory as well as the nonlinear stress-strain relations, the load-deformation curves of the short SMA columns have been predicted by using the FEM code ANSYS. Precise and quantitative analyses of these results verify the fact that the SMA column's behavior can be attributed to the special nature of the stress-strain curves.

**Keywords:** short SMA columns, two modes of deformation, two peak loads, physical nonlinearity, geometrical nonlinearity.

## 1. Introduction

Shape memory alloy (SMA) columns can exhibit unique behavior unlike the columns made of traditional materials (Rahman *et al.*, 2001; Urushiyama *et al.*, 2000). For example, Urushiyama *et al.* (2000) showed by experimental evidence that short columns made of the Cu based SMA carry higher buckling loads compared to the steel columns. It was also found that when subjected to axial compression, the curved SMA columns have the tendency to become straight before buckling. Again, Rahman *et al.* (2000; 2001) extensively demonstrated the unique buckling and postbuckling behavior for the superelastic SMA columns (sometimes termed only as SMA columns hereafter). For example, it was observed from the equilibrium configuration path that: (1) for a decreasing value of the slenderness ratio, the buckling load of the SMA column increases most significantly and below certain slenderness ratio it is higher than that of the SUS304 column. The slender superelastic SMA columns, however, buckle elastically at slightly low loads in comparison with the Al columns. (2) For higher slenderness ratio, they can sustain the load with least change in the magnitude for the postbuckling compression. (3) For a particular range of slenderness ratio, they exhibit an increase of the recovery force during unloading. (4) The residual strain is very small and thus almost the original shape of a slender column is recovered by unloading. (5) Finally, perhaps the most striking observation was- a short SMA column can exhibit two unique peaks of (buckling) load, the second peak being higher than the first one.

---

[*] To whom correspondence should be addressed

Later on, Rahman *et al.* (2005) carried out numerical simulations only for the slender SMA columns, in order to explain this unique behavior. Furthermore, Rahman *et al.* (2006) also studied the buckling of the stainless steel columns by similar experiment and numerical simulations.

It was concluded that the best results from numerical simulation would be possible, particularly for the short SMA columns, if both the tensile and compressive stress-strain curves can be considered simultaneously (Rahman *et al.*, 2005).

Since the numerical simulation was not carried out previously for the short SMA columns and tension-compression asymmetry was not considered during simulation, the present study is therefore devoted to studying these factors. In particular, taking into account both the geometrical and physical nonlinearities, an attempt is made here for the quantitative analysis of the short SMA columns.

Shape memory alloys, also termed functional materials, show two unique capabilities, that is, the shape memory effect (SME) and superelasticity (SE), which largely depend on the solid-solid, diffusion-less phase transformation process known as the martensitic transformation, from a crystallographically more ordered parent phase (austenite) to a crystallographically less ordered product phase (martensite).

The phase transformation (from austenite to martensite or vice versa) is typically marked by four transition temperatures, named martensite finish $(M_f)$, martensite start $(M_s)$, austenite finish $(A_f)$, and austenite start $(A_s)$. Let us assume, $M_f < M_s < A_s < A_f$. For $T > A_f$, the SMA exists in the parent austenite phase. Under mechanical loading the SIMT starts when a critical stress is exceeded. When the SIMT is over, the SMA exists in the martensite phase. This SIM phase is, however, unstable in the absence of stress at this temperature. Consequently, during unloading, again at a critical stress, the reverse phase transformation starts (from the SIM to parent phase) and when it is complete the SMA returns to its parent austenite phase. The complete loading-unloading cycle shows a typical hysteresis loop (Fig.1), known as pseudo-elasticity or superelasticity. The SIMT and the reverse SIMT are marked by a reduction of the material stiffness (Fig.1).
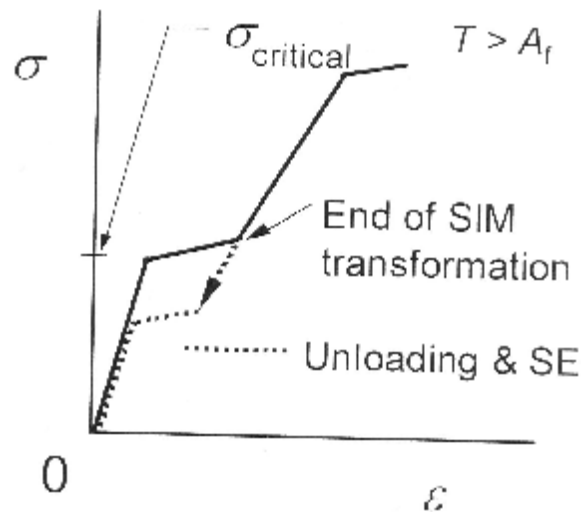


Fig.1. Idealized stress-strain diagram of the superelastic SMA.

For $T < A_s$ there is no pseudoelastic recovery and the residual strain can be recovered by heating above $A_f$ (SME). For any temperature there exists a critical stress for irreversible plastic slip to occur in the material (this critical stress value decreasing with increasing temperature), and if the stress is exceeded, then the residual strain cannot be recovered by heating or unloading. At room temperatures, usually, the superelastic Nitinol SMA can fully recover up to *6.5%* strain as pointed out in Rahman (2001).

The following paragraphs give brief descriptions of the relevant terms, like structural (geometric and material) nonlinearity and also the effect of structural nonlinearity on the buckling and postbuckling equilibrium configuration paths of a structure.

## 2. Equations for nonlinear structural analysis

As far as the deformation of an ideal simple column is concerned, it can be shown that if only the geometric nonlinearity is taken into considerations, the load-deflection curve becomes convex upward.

On the other hand, in order to demonstrate the effect of nonlinear material stiffness on the equilibrium path, the simple and ideal elastic system shown in Figs 2-3 can be analysed (Norris and Wilbur, 1960). The compressed rod of length $L$ is perfectly rigid and nondeformable. The only way that the system can deflect is for the spring to elongate. The spring has bi-linear stiffness. That is, given, $\lambda = L\theta$, and $\lambda_1 = L\theta_1$ the stiffness of the spring reduces from $K$ to $k$ if its elongation exceeds $\lambda_1$.
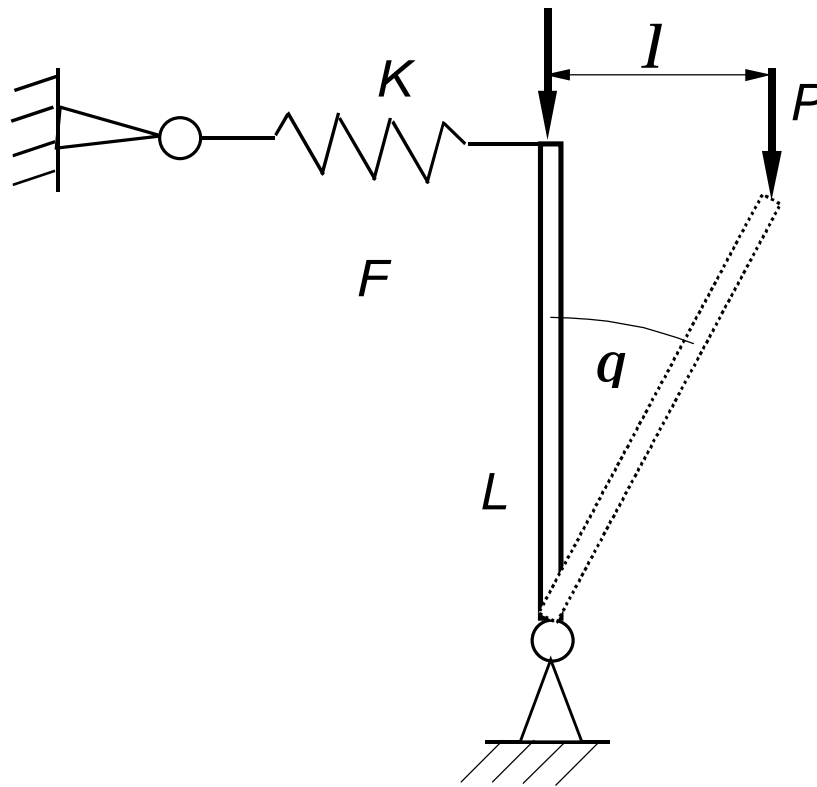


Fig.2. Buckling of an ideal elastic model.

The critical load corresponding to the buckling condition that is, $P_{cr} = KL$, can be identified simply by studying the characteristics of the equilibrium configuration path (load-deflection curve) for the system.

As $P$ approaches $P_{cr}$ the deflection becomes boundless as shown by the solid straight line of Fig.3. In terms of bi-linear spring behavior, the stiffness reduces to $k$ as the spring force exceeds $k\lambda_1$ or, $kL\theta_1$. For such a spring the above equations are valid only up to the point where $\theta$ equals, $\theta_1$. If the deflection exceeds $\theta_1$, the following equations would give $P_{cr}$

$$F = KL\theta_I + kL(\theta - \theta_I),$$ (2.1)

and $$P = KL\theta_I/\theta + kL(1 - \theta_I/\theta).$$ (2.2)

When the spring force reaches $KL\theta_I$, the load deflection curve breaks down sharply and becomes asymptotic to the horizontal line corresponding to $P = kL$. Importantly, for the present study, the stress-strain curve of the SMA is highly nonlinear, analogous to such a spring with variable stiffness.
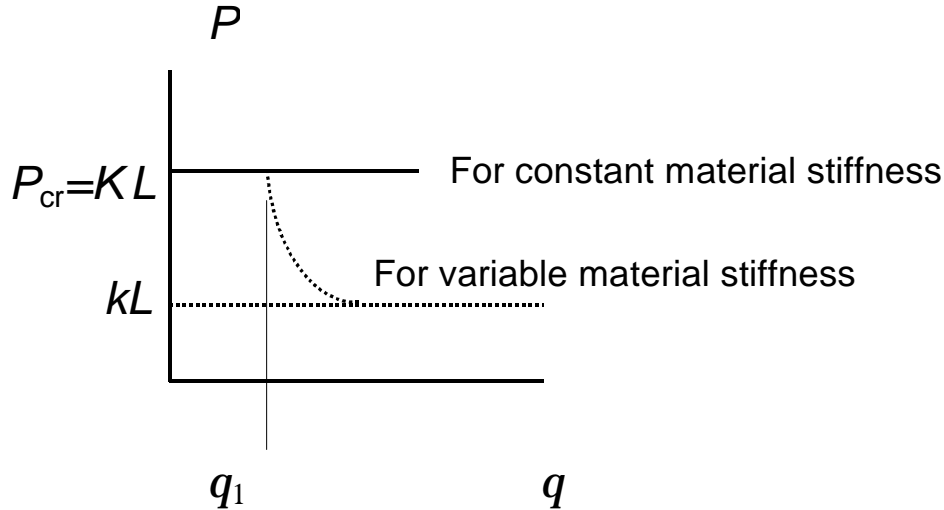


Fig.3. Equilibrium configuration paths for the ideal elastic model of Fig.2 with nonlinear material stiffness.

## 3. Test conditions and experimental procedure

The materials, configurations and conditions used in this experiment were as follows. Column materials: SMA (Ti49.3 at% Ni50.2at% V0.5at%), stainless steel (SUS304), and aluminum. The unsupported column lengths were *14* and *19* (*mm*), while the diameter was *2mm*. SMA's transformation temperatures were, $-59\,^{\mathbf{o}}C$, $-34\,^{\mathbf{o}}C$, $-27\,^{\mathbf{o}}C$ and $-3\,^{\mathbf{o}}C$ for $M_f$, $M_s$, $A_s$ and $A_f$, respectively. The room temperature range was $23\,^{\mathbf{o}}C - 30\,^{\mathbf{o}}C$. An instron machine was used and the speed of the cross-head during loading-unloading cycle was so adjusted that the strain rate was *0.10*/min .

At first, the columns were inserted into the holes of the loading fixtures (Fig.4). During loading, the moving fixture moved towards the fixed one until its predetermined final position $(\Delta_{set})$ was reached. In the meantime, the column buckled and had enormous deformations. Immediately after the final point of displacement was reached, the moving fixture was moved away from the fixed one, allowing the largely deformed column to gradually recover its shape. The unloading process was stopped and the cycle ended when *P* became approximately zero (Fig.5). The values of $\Delta_{set}$ were *10%* and *5.5%*, for the columns with $L/k = 28$ and *38*, respectively, in order to closely observe the interesting $P - \Delta$ curves.

Practically, it is difficult to fully eliminate the gap that remains between the loading fixture and the column at the beginning of the loading; this gap will affect the displacement reading of the $P - \Delta$ curve of the experimental data. Of course, the load-cell reading is more important as far as buckling is concerned and it remains unaffected by the displacement reading.
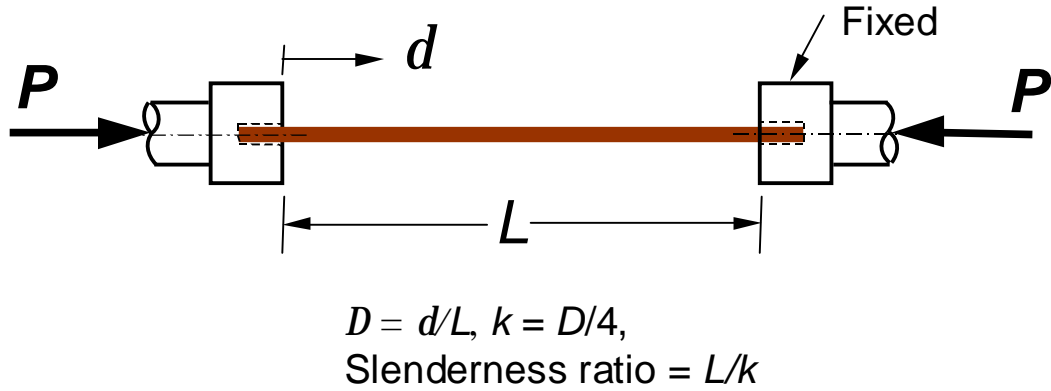
$$D = d/L,\ k = D/4,$$
$$\text{Slenderness ratio} = L/k$$

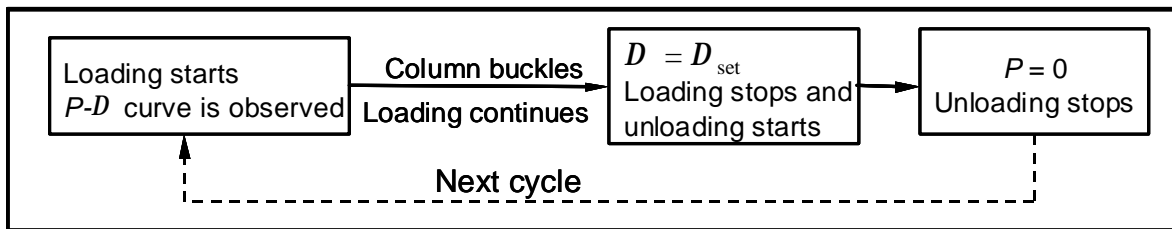Fig.4. Column inserted into the fixture.



Fig.5. Experimental procedure.

## 4. Simulation scheme

A static analysis has been performed by the commercial FEM code ANSYS (Swanson Analysis Systems, Inc.), using the half model of the column, as shown in Fig.6. Details of the modelling are explained in the appendix. A negligibly small transverse disturbance, necessary for buckling analysis, was assigned by $F_y$ (the magnitude was *1N*) at any point on the mid-span of the column.
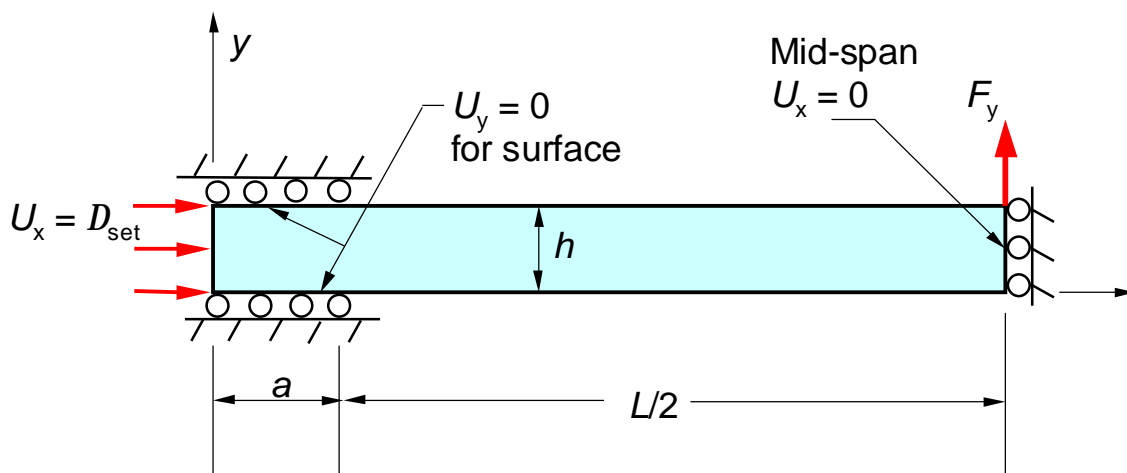


Fig.6. Half model of the column used for simulation.

During loading (in terms of $\Delta$), the total end displacement $\left(\Delta_{set}\right)$ was assigned in a sufficiently large number of steps for accurate calculation of the buckling load.

The stress-strain (some times abbreviated as $s-s$ in this paper) curves for the superelastic SMA are determined by experiment for sufficiently large strain (Fig.7) and used for the simulation. Poisson's ratio, density and Young's modulus were found to be *0.33*, $6.5 \times 10^3 \, kg/m^3$ and $65 \times 10^9 \, Pa$, respectively for SMA.
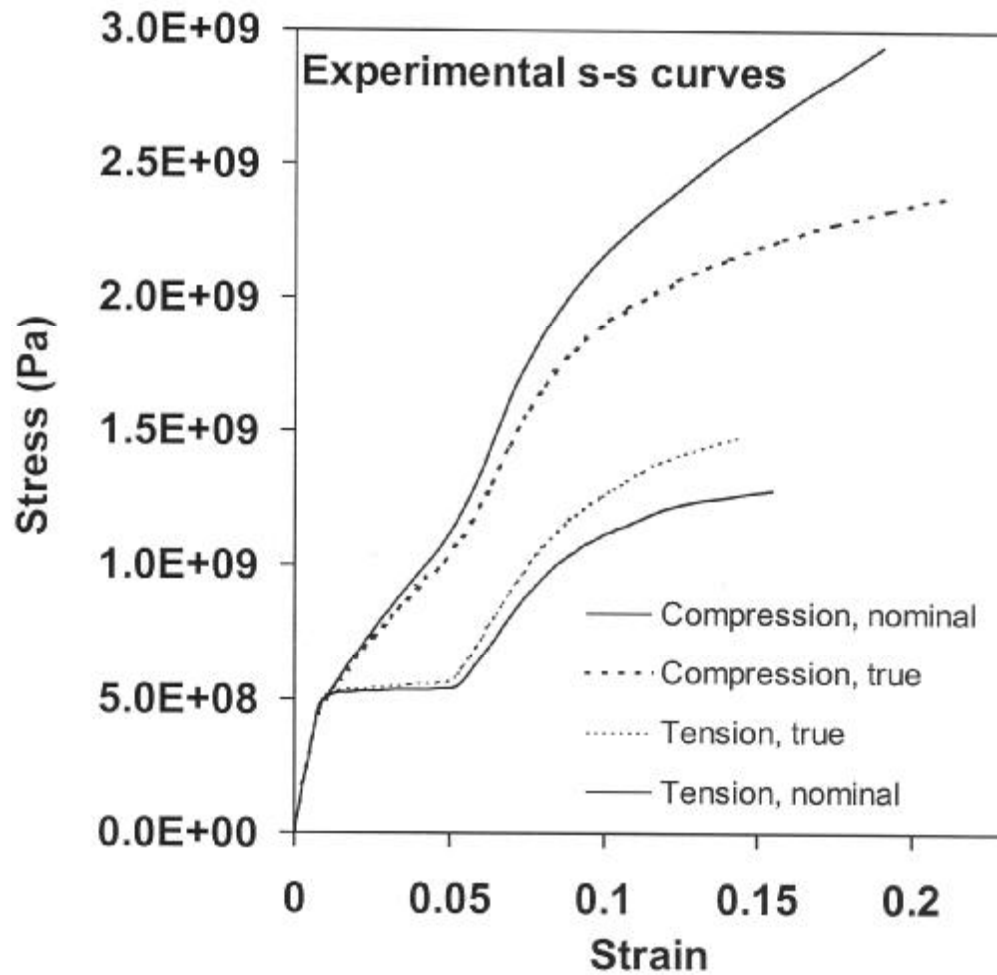


Fig.7. Experimental stress-strain curves for the superelastic SMA ( $D = 2mm$ ).

The present simulation scheme uses the following two different kinds of material models.

Mooney-Rivlin (M-R) or the Hyperelastic model- Hyperelasticity refers to materials whose stresses are derived from their total strains using a strain energy density function. M-R is a material law suitable for nearly incompressible natural rubber. For this model, both the tensile and compressive stress-strain data can be used simultaneously.

The multilinear elastic (MELAS) model- suitable for large strain-this can accurately represent the highly nonlinear material behavior by a piece-wise-linear curve, through at most *100* stress-strain points. The compressive and tensile $s-s$ data can not be used simultaneously. Since the present study is concerned with only the equilibrium configuration paths of the short SMA columns during loading, interested readers may

refer to Rahman (2001) and Rahman *et al*. (2005), regarding how this model was used to simulate the complete loading-unloading cycle for the slender superelastic SMA columns.

## 5. Results and discussion

### 5.1. Short SMA column's unique buckling behavior – qualitative analysis

As observed, for the SMA column with $L/k = 28$, the load increases after a distinct change in the mode of deformation (Fig.8). It should be noted that the term 'change in the mode of deformation' is used here to refer to the distinct change in the slope of the $P - \Delta$ curve for a column. The portion of the $P - \Delta$ curve connecting the two modes of deformation contains a point of instability, according to Thompson and Hunt (1973). As seen, unlike the Al and SUS304 columns, quite remarkably, this SMA column can sustain a significantly high load during its secondary mode of deformation (Fig.8).
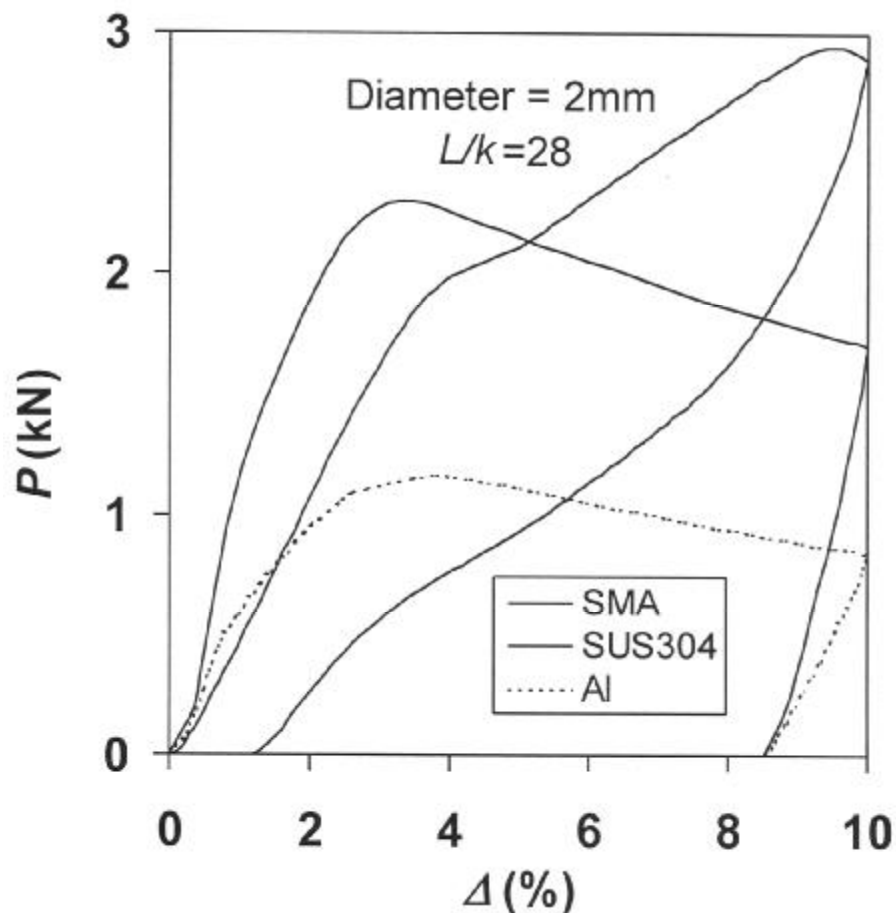
Fig.8. Experimental load-end shortening curves for $L/k = 28$ (After, Rahman *et al*., 2001).

On the other hand, for $L/k = 38$, the $P - \Delta$ curve of the SMA column (Fig.9) shows a valley between two distinct buckling loads (the second peak being slightly higher than the first one). The above characteristic is contrary to the general trend that load falls off monotonously, for any further compression, after the first distinct buckling load on the equilibrium configuration path of a column.
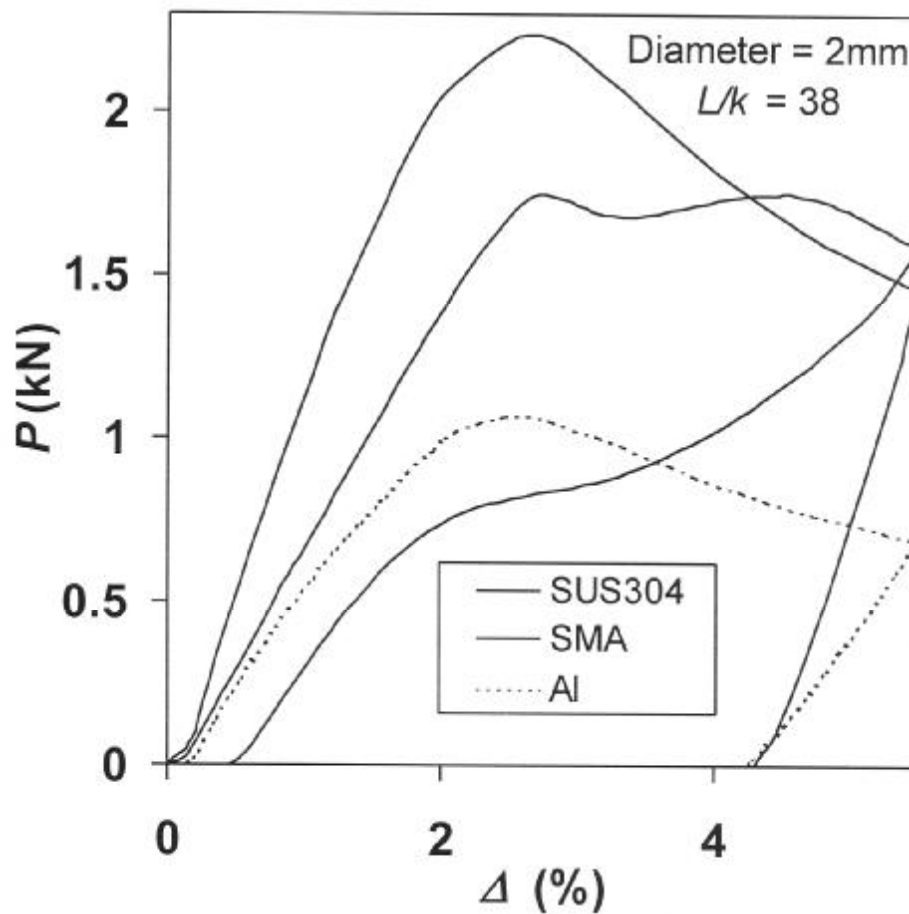
Fig.9. Experimental load-shortening curves for $L/k = 38$ (After, Rahman *et al*., 2001).

Because of large deformation (compression plus bending) the SIMT is initiated within the column material. As seen from Fig.7, unlike the tensile $s - s$ curve, there is no distinct plateau during the SIMT process for the compressive $s - s$ curve. Rather the initiation of the SIMT may be marked by a slight and smooth decrease in the material stiffness. It appears, because of this decrease in the material stiffness, the highly compressed SMA column (which is prone to buckling if there is any kind of disturbance) gradually approaches the first point of instability with increasing value of end shortening. After the SIMT is completed, the material stiffness again increases significantly (Fig.7), which in turn increases the resisting moment of the bent column. Consequently, during the secondary mode of deformation, the bending effect due to the applied load is overcome by the resisting moment until the second point of instability is reached (Figs 8, 9), as pointed out in the previous experimental study (Rahman *et al*., 2001).

### 5.2. Simulated equilibrium configuration paths – quantitative analysis

The simulation results for the SMA columns with $L/k = 28$ show that the MELAS model using the pure compressive stress-strain curve can predict the column's peak or, the higher buckling load most accurately (Fig.10). On the other hand, the predicted load-end shortening curve based on the tensile $s - s$ data, dips a little to a valley and again rises to a higher peak, which remains much lower than the

experimental result. The reason can be explained while analyzing the total strain distribution in the same column (Fig.11). The initial portions of the $P-\Delta$ curves predicted by the MELAS model merge together while those predicted by the M-R model show less stiffness (Fig.10). This is because the input s-s curves are slightly modified while the M-R model is used.

The M-R model predicts a much lower buckling load than the experimental result as can be seen from Fig.10. This is due to an interesting phenomenon, that is, the change in the mode of deformation (after the first point of instability, corresponding to a load of *1.92kN*) on the $P-\Delta$ curve of this column. Incidentally, at this point, the theorems of Thompson and Hunt (1973) seem to apply perfectly. The theorems state that the onset of first point (either a limit point or a branching point) of instability is indicated by a substantial increase in the displacements for very a small increase of the loading parameter, and thus the numerical technique fails to converge to any solution.
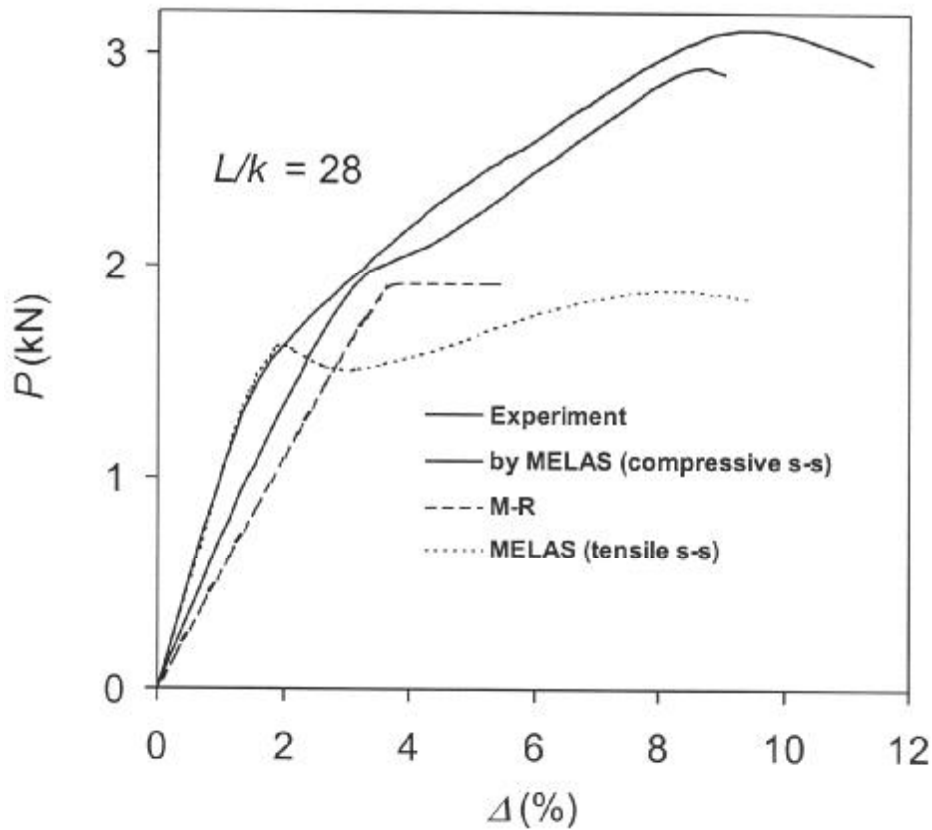


Fig.10. Load-end shortening curves (experiment and simulation) for the SMA column.

The distribution of total strain (in the loading direction), corresponding to the critical state, over the entire half-model of the column, is as shown in Fig.11. This strain distribution should be observed in conjunction with the stress-strain curves (Fig.7) and also the load-deformation curves (Fig.10). As seen, most of the column material is under compression and the maximum compressive strain is as high as *12.2%* (Fig.11), which justifies the use of only the compressive stress-strain curve for simulation. The maximum tensile strains (*1.68%*) occur in the small regions. Since the asymmetric tension-compression behavior of the SMA is significant particularly beyond *1%* strain, the simulation result based only on the compressive stress-strain curve (MELAS model) can be used reliably to predict the buckling behavior for such a short column.
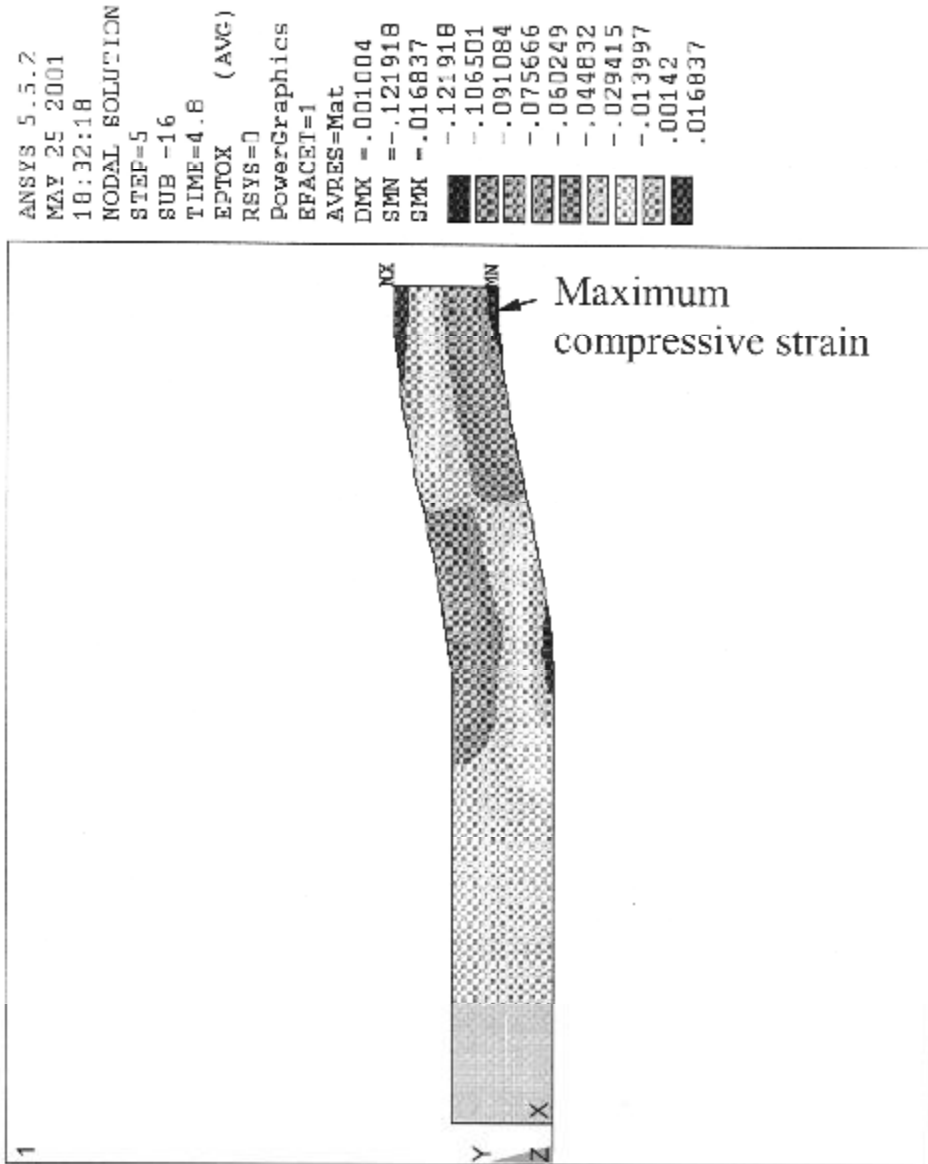
Fig.11. Total strain distribution in the loading direction for the SMA column $(L/k = 28)$ based on the MELAS model and compressive $s - s$ curve corresponding to the critical point $(\Delta = 9.4\%)$.

Because of large strains (over $6.5\%$) some parts of this column (Fig.11) will induce permanent deformations upon unloading as evidenced by the residual strains shown by the experimental results of Figs 8 and 9.

For $L/k = 38$, both the MELAS model (based on the compressive stress-strain data) and the M-R model can predict the $P - \Delta$ curve, including the buckling load, though the valley between the two peaks can not be predicted, as shown in Fig.12. It appears that both the tension and compression stress-strain curves of SMA are responsible for such a valley, and only a material model similar to the MELAS model but capable of handling tension-compression asymmetry can predict the valley between the two unique peak loads. The

M-R model predicts a distinct bifurcation point at a position corresponding to the valley of the load-deformation curve but the load falls during the secondary mode of deformation.
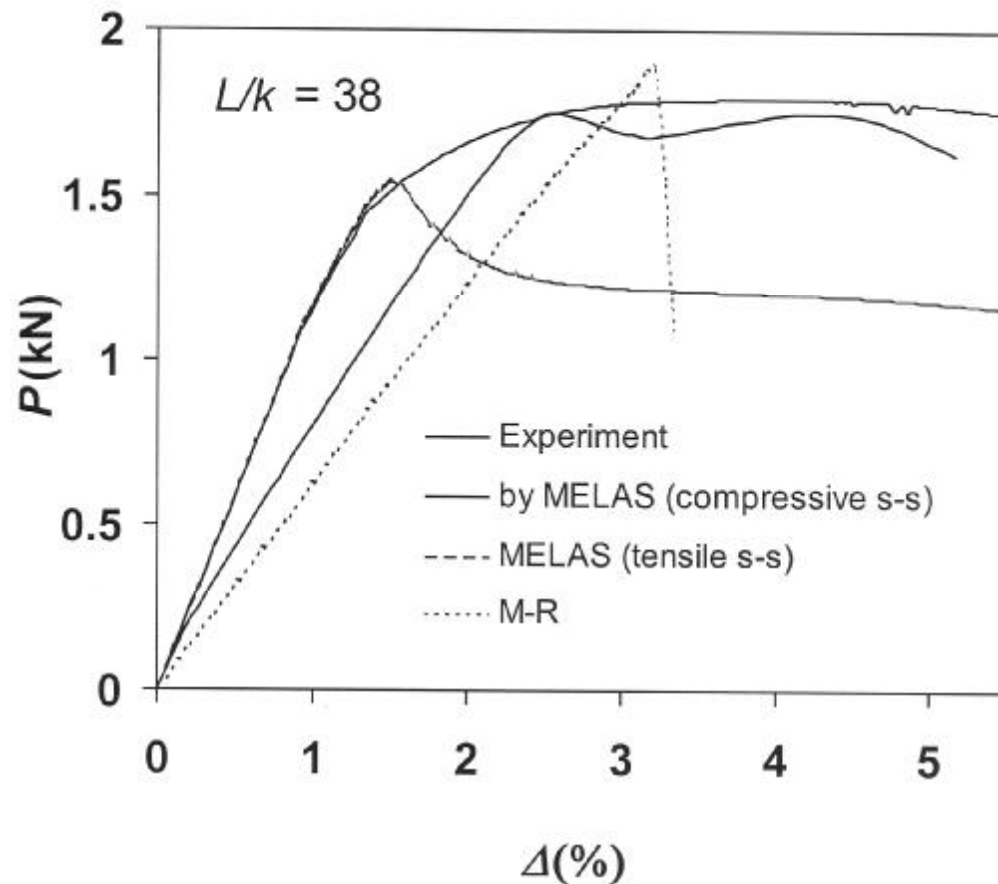


Fig.12. Load-end shortening curves (experiment and simulation) for the SMA column.

### 5.3. Accuracy of the results

The easiest way to check the accuracy of the presented results is to make use of the famous Euler's formula ($4\pi^2\,EI/L^2$, symbols having their usual meanings) for both ends-clamped slender SMA columns. Using this strategy it was shown in Rahman *et al*. (2005) that the experimental buckling loads are very close to their theoretical values, according to the above formula. For ready reference, Fig.13 is presented. It is interesting to note that because of superelastic shape recovery, the force increases remarkably during unloading of this slender SMA column (Fig.13). For this slender SMA column, the experimental buckling load is *234N* and Euler's formula $\left(E=65\,GPA\right)$ gives a load of *285.2N*, while from simulation results based on MELAS model using compressive stress-strain curve gives a buckling load of *260.7N* which is closer to the experimental result. This simple comparison in turn verifies the soundness of the same simulation scheme applied to the short SMA columns for the present analysis.
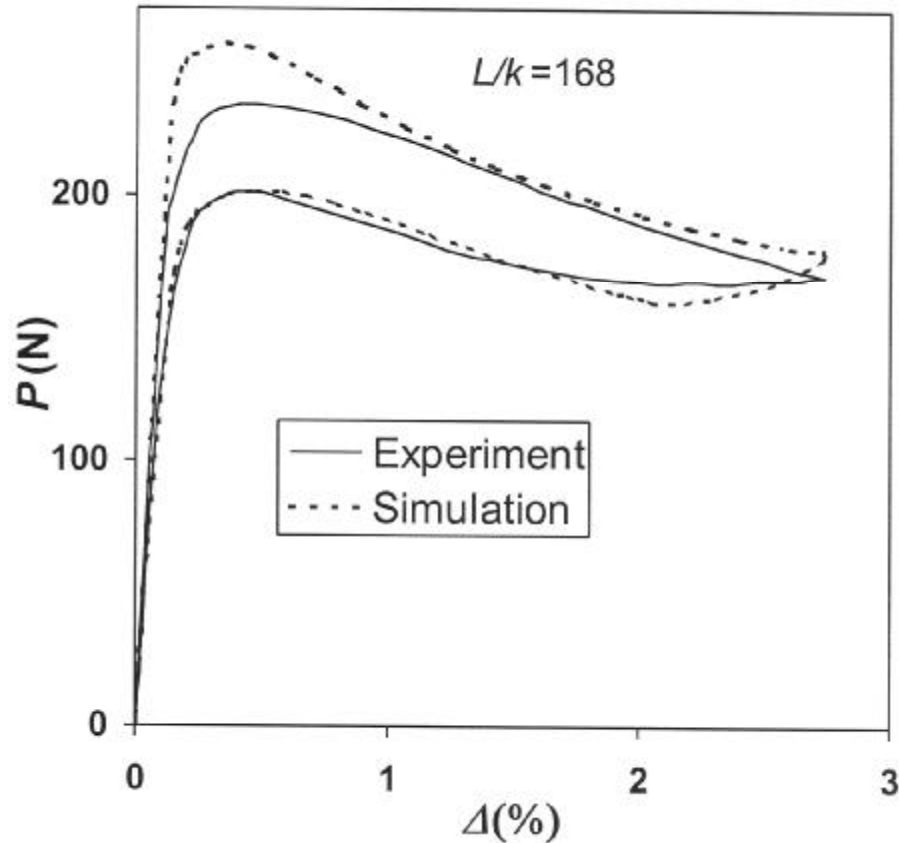
Fig.13. Load-end shortening curves for a complete cycle (experiment and simulation) for $L/k = 168$ for the SMA column using MELAS model and compressive $s - s$ curve (After, Rahman *et al.*, 2005).

## Conclusions

Using a loading-unloading cycle, some interesting and useful buckling and postbuckling characteristics of the superelastic SMA columns were observed experimentally. Those phenomena depend largely on the slenderness ratio. For example, the $P - \Delta$ curve for the short SMA column with $L/k$ of *38* shows two distinct peak loads during loading, the other one being higher, quite contrary to the general notion that load falls off monotonously for other columns during any further compression beyond the first peak load. Similarly, for $L/k$ of *28*, the SMA column can sustain significantly high load (even higher than that of a SUS304 column) after a distinct change in the mode of deformation. Thus the short superelastic SMA columns can be excellent candidates for any engineering application where high compressive load carrying capability is required for a few repeated loading-unloading cycles.

A comprehensive simulation scheme has been used incorporating both the physical and geometrical nonlinearities in order to predict the equilibrium configuration paths along with the total strain distributions in the column materials at different states of loading.

In general, present analyses of the results verify the fact that the SMA column's unique behavior could be attributed mainly to the special nature of the stress-strain curves far beyond the region of SIMT. During quantitative analysis, theorems of Thompson and Hunt are found to be useful

to predict the unique first point of instability of the short SMA columns. A comparison shows the simulation scheme used here can predict the experimental buckling load better than theory.

## Nomenclature

$F_y$ – perturbing force applied on the mid-span of the model
$k$ – least radius of gyration of the cross sectional area
$L$ – unsupported length of the columns at $P = 0$
$P$ – axial compressive load
$U_x, U_y$ – nodal displacements for the model in the *x* and *y* directions, respectively
$\delta, \Delta$ – displacement of the moving fixture, $\delta/L$

## Appendix

### Simplified column model

For simulation, the element type used for the MELAS model was PLANE42 (4 nodes, 2-D space, DOF: UX, UY), while for the M-R model, the element type was HYPER56 (hyperelastic mixed U-P solid, 4 nodes, 2-D space, DOF: UX, UY, UZ).

Theoretically, linearly elastic columns having the same slenderness ratio and same cross-sectional area (but perhaps of different shapes) will exhibit the same buckling characteristics. For a circular cross-sectional area, the least radius of gyration is, $k_c = D/4$. For a rectangular cross-sectional area, with its sides *b* and *h* $(b > h)$, the least radius of gyration is, $k_r = h/3.4641$. For the present study, $D = 2mm$. Thus, having the same length, the slenderness ratio and area will be the same for the circular cross-sectional area and a rectangular cross-sectional area, if, $h = 1.732mm$ and $b = 1.814mm$. The geometric half model of the column (with $h = 1.732mm$, and $b = 1.814mm$ in the *z*-direction), as represented in Fig.7, is used for the purpose of simulation. The length of the column inserted between the fixture, that is, the value of *a* was *8mm* (Fig.7) and the element size for the finite element meshing was *0.20mm*. High accuracy of the results using this half model of column can be checked from the present study and also from Rahman *et al*. (2005; 2006). For more precise quantitative analysis of nonlinear structural behavior, however, it is important to model the exact correct cross-sectional shape (that is the round circular cross-section).

### True and nominal stress-strain curves

For accuracy of the simulation involving large strains, the nominal stress-strain curve was changed to the true stress-strain curve. It should be noted that the characteristic plateau for the SIMT in tension, as well as the tension-compression asymmetry, starts when the strain is approximately *1%*. The entire tensile strain data was measured by the strain gage. On the other hand, following Johnson (1972), to avoid any chance of bending/buckling of the specimen during the pure compression test, $L/k$ was kept less than *12*. Thus, strain gage could not be used because of too small gage length $(4.5mm)$ of the

test specimen during the compression test and the strain data were measured only by the displacement of the moving fixture. However, the accuracy of simulation results largely depends on the correct stress-strain data. Particularly, for simulating the behavior of the columns that are not too short, at least the initial portion of the stress-strain should be highly accurate. Thus to compromise, while keeping continuity of the data, only the initial portion (*0* to about *1%* strain) of the compressive stress-strain curve, was modified to make it identical with the tensile stress-strain curve, until the distinct plateau for the SIMT in tension is approached (Fig.7). It is found that based on the modified compressive stress-strain data, the buckling and postbuckling behavior of the SMA columns can be predicted with reasonable accuracy for any *L/k* (Rahman *et al*., 2005).

For the M-R hyperelastic model, the nominal stress-strain data are required as input. ANSYS software at first calculates the 2 terms, 5 terms or, the 9 terms Mooney-Rivlin constants (strain energy constant) from the given stress-strain data. Next, based on these constants, the stress-strain data are modified. There is no fixed rule for selecting the number of strain energy constant terms. However, modified data, which suit the actual data best in tension and compression, should be chosen. Since the 9 terms M-R constants show a better match with the experiment, only the load-deformation curves traced by 9 terms constants are presented here (Fig.14). Moreover, this model is suitable for incompressible natural rubber and recommends Poisson's ratio of *0.499*. It was found that the SMA column's buckling load increases if the Poisson's ratio is chosen as *0.499* instead the actual value of *0.33*. To minimize the number of figures, however, those simulation results are not shown in this study. Interested readers may refer to Rahman (2001) for more details.
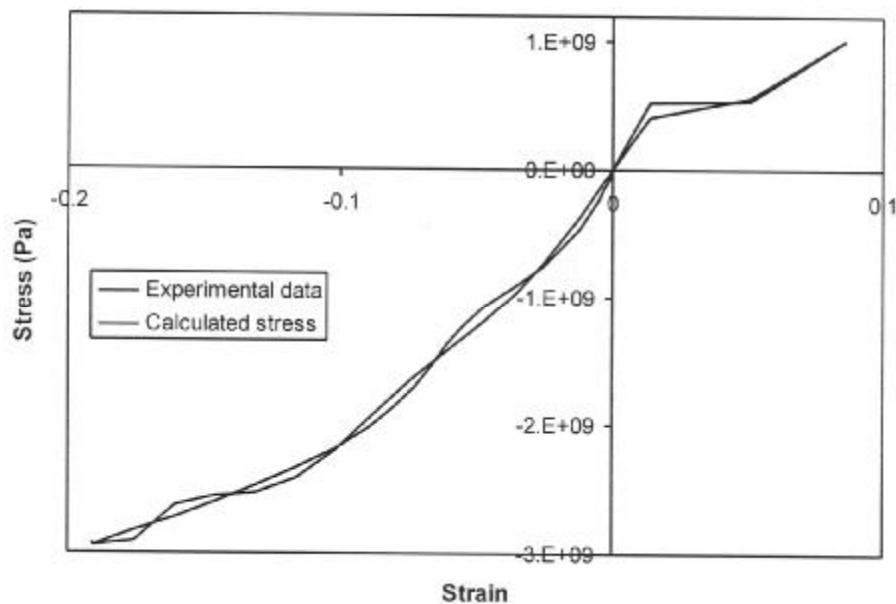


Fig.14. Calculated stresses based on 9 terms Mooney-Rivlin constants.

## References

Johnson W. (1972): *Impact strength of materials*. – Edward Arnold.

Norris C.H. and Wilbur J.B. (1960): *Elementary structural analysis.* – McGraw-Hill Book Company.

Rahman M.A. (2001): *Behavior of the superelastic shape memory alloy columns under compression and torsion.* – Ph D Thesis, Tohoku University, Japan.

Rahman M.A., Qiu J. and Tani J. (2000): *Behaviors of the superelastic SMA columns under compressive loading-unloading cycles.* – Proceedings of the 11th International Conference on Adaptive Structures and Technology (Nagoya, Japan), pp.351-358.

Rahman M.A., Qiu J. and Tani J. (2001): *Buckling and postbuckling characteristics of the superelastic SMA columns.* – International Journal of Solids and Structures, vol.38, pp.9253-9265.

Rahman M.A., Qiu. J. and Tani. J. (2005): *Buckling and postbuckling characteristics of the superelastic SMA columns-Numerical Simulation.* – Journal of Intelligent Material Systems & Structures, vol.16, pp.691-702.

Rahman M.A., Tani J. and Afsar A.M. (2006): *Postbuckling Behaviour of Stainless Steel (SUS304) Columns Under Loading-unloading Cycles.* – Journal of Constructional Steel Research (In press).

Thompson J.M.T. and Hunt G.W. (1973): *A General Theory of Elastic Stability.* – UK, John Wiley and Sons.

Urushiyama Y., Lewinnek D., Qiu J. and Tani J. (2000): *Buckling of curved column and twinning deformation.* – Abstracts of the IUTAM Symposium on Smart Structures and Structonic Systems, pp.38-39.